

Effects of Halo Substructure on the Power Spectrum and Bispectrum

Derek Dolney,^{*} Bhuvnesh Jain,[†] Masahiro Takada[‡]

Department of Physics and Astronomy, University of Pennsylvania, 209 S 33RD ST, Philadelphia, PA 19104-6396, USA

2 December 2024

ABSTRACT

We study the effects of halo substructure and a distribution in the concentration parameter of haloes on large-scale structure statistics. The effects on the power spectrum and bispectrum are studied on the smallest scales accessible from future surveys. We compare halo model predictions with results based on N -body simulations, but also extend our predictions to 10-kpc scales which will be probed by future simulations. We find that weak lensing surveys proposed for the coming decade can probe the power spectrum on small enough scales to detect substructure in massive haloes. We discuss the prospects of constraining the mass fraction in substructure in view of partial degeneracies with parameters such as the tilt and running of the primordial power spectrum.

Key words: cosmology: dark matter – halo model – substructure

1 INTRODUCTION

The substructure of dark-matter haloes is a topic of interest in cosmology, especially due to its relevance to the cold dark matter model, which requires some degree of clumpiness to the matter distribution. In a recent paper, Kochanek & Dalal (2003) argue that substructure provides the best explanation (originally proposed by Mao & Schneider 1998) of the anomalous flux ratios found in gravitational lens systems. However, the observed number of dwarf galaxy satellites in the Local Group is more than an order of magnitude smaller than the number of subhaloes found in numerical simulations (Klypin et al. 1999; Moore et al. 1999b).

Observable statistics of the matter distribution provide an approach to substructure studies that is complementary to studies of strong lens systems or direct observations of satellite galaxies. Substructure effects are expected to produce an observable effect in the power spectrum in the next generation of lensing surveys. As we show in this paper, substructure effects in the weak-lensing regime probe cluster scales primarily, as opposed to strong-lensing systems, which probe galactic scales.

The halo model provides a description of non-linear gravitational clustering which allows statistical quantities of interest to be efficiently computed. The essential concepts of the halo model were used by Neyman & Scott (1952)

to describe the spatial distribution of galaxies over fifty years ago. Their results were later generalized by Scherrer & Bertschinger (1991). By combining the formalism of Scherrer & Bertschinger with results from N -body simulations such as a halo density profile (e.g., that of Navarro, Frenk & White 1997) and a halo mass function and bias parameters (e.g, Sheth & Tormen 1999), one is able to calculate various dark-matter and galaxy clustering statistics (Seljak 2000; Ma & Fry 2000; Scoccimarro et al. 2001; Cooray & Hu 2001). See Cooray & Sheth (2002) for a comprehensive review of the halo model.

Most work on the halo model approximates haloes as spherically symmetric objects, described by a mass density which is a smoothly decreasing function only of the distance from the halo centre. However, the density distribution of haloes which form in N -body simulations is not at all smooth (Navarro et al. 1997; Moore et al. 1999a). Rather, one finds that about ten percent of the mass is associated with subhaloes (Tormen, Diaferio & Syer 1998; Ghigna et al. 2000). In the large-scale structure literature to date, the effects of halo substructure are typically assumed to be small for purposes of calculating statistics of the dark matter distribution. This paper explores the validity of this assumption. We will make quantitative statements about the size of substructure effects on the 2-D and 3-D dark-matter power spectra and bispectra. We will identify the length and angular scales at which halo substructure becomes important.

The results of N -body simulations also suggest a distribution of halo concentration parameters (Bullock et al. 2001; Jing 2000). Like substructure, this effect is often ignored,

^{*} email: dolney@astro.upenn.edu

[†] email: bjain@physics.upenn.edu

[‡] email: mtakada@hep.upenn.edu

though the formalism to include it in the halo model is straightforward (Cooray & Hu 2001). This paper will quantify the effect of a concentration parameter distribution on the power spectra.

2 THEORY

To model substructure in a halo, the total mass M of the halo is divided into a smoothly-distributed component of mass M_s , and the remaining mass m is placed in subhaloes. Ignoring substructure, the halo model requires specification of the halo density profile and the mass function, i.e., the number density of haloes of a given mass. To include substructure, one must specify not only the density profile of the smooth component, the Fourier transform of which we denote $M_s U(k; M_s)$, but also the density profile of the subhaloes, with Fourier transform $m u(k; m)$. The mass factors simply provide the proper normalization; $U(k; M_s)$ and $u(k; m)$ are normalized to unity. Suitable mass functions for the number density both of parent haloes, dN/dM , and of subhaloes, dn/dm , are also needed. In addition, the distribution of subhaloes within the parent halo must be specified. We denote its Fourier transform by $U_c(k; M_s)$. Using these ingredients, Sheth & Jain (2003) derive expressions for the power spectrum and the bispectrum. We give some results from their paper that are relevant to this work in the Appendix.

We use the mass function of Sheth & Tormen (1999) for the number density of parent haloes of a given mass M :

$$dM \frac{dN(M)}{dM} = \frac{\bar{\rho}}{M} A [1 + (a\nu)^{-p}] \sqrt{a\nu} e^{-a\nu/2} \frac{d\nu}{\nu}, \quad (1)$$

where $\bar{\rho}$ denotes the average density of the universe at the present epoch, and

$$\nu(M, z) := \left[\frac{\delta_c(z)}{D(z)\sigma(M)} \right]^2 \quad (2)$$

is the peak height defined in terms of $\delta_c(z)$, the threshold overdensity in the spherical collapse model, $D(z)$, the growth factor for density perturbations, and $\sigma(M)$, the rms fluctuations in the matter density field at the present epoch smoothed with a top-hat window of radius $(3M/4\pi\bar{\rho})^{1/3}$. For δ_c , we use the fitting formula of Henry (2000). We use haloes with mean interior density 180 times the background density and take $a = 0.67$ and $p = 0.33$, so that our mass function is universal (White 2002). The notation of this paper reflects our choice of halo boundary: $r := r_{180b}$, $M := M_{180b}$, and $c := r_{180b}/r_s$. The normalization constant is fixed by requiring that all mass be contained within a parent halo, and turns out to be $A = 0.116$.

We assume a biasing prescription for the clustering of parent haloes. That is, the halo power spectrum is given in terms of the linear mass power spectrum $P_L(k)$ as:

$$P(k, z; M_1, M_2) = b_1(\nu_1) b_1(\nu_2) P_L(k, z), \quad (3)$$

where $\nu_i := \nu(M_i, z)$. We use the bias parameter of Sheth & Tormen (1999):

$$b_1(\nu) = 1 + \frac{a\nu - 1}{\delta_c} + \frac{2p/\delta_c}{1 + (a\nu)^p}. \quad (4)$$

For the subhaloes, we assume a power-law distribution

suggested by numerical simulations (Tormen et al. 1998; Ghigna et al. 2000):

$$\frac{dn(m; M)}{dm} dm = N_0 \left(\frac{M}{m} \right)^\mu \frac{dm}{m}, \quad (5)$$

where $\mu < 1$. The normalization N_0 is determined by the mass fraction contained in subhaloes, f :

$$f := \frac{M - M_s}{M} = \int dm \frac{m}{M} \frac{dn(m; M)}{dm}. \quad (6)$$

Numerical simulations suggest $\mu \approx 0.9$ and $f \approx 10\%$. We use these values unless otherwise noted. In addition, simulations suggest that subhaloes heavier than 1% of the total mass in the parent halo are rare (Tormen et al. 1998; Chen, Kravtsov & Keeton 2003), so we only include subhaloes with masses $m \leq 0.01M$.

We use the density profile of Navarro et al. (1997), hereafter NFW, for both the smooth component and the subhaloes. Furthermore, we assume the distribution of subhaloes within a parent halo follows the mass distribution of the smooth component. That is, $U_c(k; M_s)$ is also given by the NFW profile, normalized to unity. We use the concentration parameters found by Bullock et al. (2001), for all three profiles at redshift z , which are

$$\bar{c}(M, z) = 9(1+z)^{-1} \left[\frac{M_{\text{vir}}(M)}{M_*} \right]^{-0.13} \quad (\text{smooth}), \quad (7)$$

for the smooth component of a halo, and

$$\bar{c}(m, z) = 7.5(1+z)^{-1} \left[\frac{m_{\text{vir}}(m)}{M_*} \right]^{-0.30} \quad (\text{subhalo}), \quad (8)$$

for all subhaloes. The non-linear mass scale M_* is defined by the relation $\nu(M_*, 0) = 1$. The translation $M_{\text{vir}}(M)$ between different halo mass definitions is derived in the Appendix of Hu & Kravtsov (2003). Bullock et al. find that the concentration parameter for subhaloes has some dependence on the local density around the subhalo. We ignore this effect here, as it is difficult to include in our model, and we do not believe inclusion would seriously affect our conclusions. Huffenberger & Seljak (2003) find a different concentration parameter by χ^2 minimization against the non-linear fitting formula of Smith et al. (2003):

$$\bar{c}(M, z) = 11(1+z)^{-1} \left(\frac{M}{M_*} \right)^{-0.05}. \quad (9)$$

Numerical simulations suggest a log-normal distribution for the concentration parameter about the mean value \bar{c} :

$$p(c; m, z) dc = \frac{d(\ln c)}{\sqrt{2\pi\sigma_{\ln c}^2}} \exp \left\{ -\frac{\ln^2[c/\bar{c}(m, z)]}{2\sigma_{\ln c}^2} \right\}, \quad (10)$$

with a width $\sigma_{\ln c} = 0.3$ (Bullock et al. 2001; Jing 2000). Unless otherwise noted, we use the mean values given in Eqs. 7–8.

We calculate the weak lensing convergence using Limber's approximation (Limber 1953; Kaiser 1992), so that the convergence power spectrum and bispectrum are given by

$$P^\kappa(l) = \int_0^{\chi_s} d\chi \frac{W^2(\chi)}{d_A^2(\chi)} P \left(\frac{l}{d_A(\chi)} \right), \quad (11)$$

$$B^\kappa(l_1, l_2, l_3) =$$

$$\int_0^{\chi_s} d\chi \frac{W^3(\chi)}{d_A^4(\chi)} B\left(\frac{l_1}{d_A(\chi)}, \frac{l_2}{d_A(\chi)}, \frac{l_3}{d_A(\chi)}\right). \quad (12)$$

In the next section we will also use the reduced bispectrum, defined as $B/3P^2$ for equilateral triangles.

We use the standard weak lensing weight function (see, e.g., Bartelmann & Schneider 2001)

$$W(\chi) = \frac{3}{2} \Omega_m H_0^2 a^{-1} \frac{d_A(\chi) d_A(\chi_s - \chi)}{d_A(\chi_s)}, \quad (13)$$

where χ is the comoving distance, χ_s is the comoving distance of the source galaxies, and $d_A(\chi)$ is the comoving angular diameter distance, and H_0 is the present-day value of the Hubble parameter. For simplicity, we place all source galaxies at redshift one.

We will calculate the covariance of the convergence field by adopting a binning scheme. Let P_i^κ denote the power averaged over a bin of width Δ_i centred on the mode l_i . Our bins are chosen to have width $\Delta_i/l_i = 0.3$. In this notation, the covariance can be expressed as (Cooray & Sheth 2002; Meiksin & White 1999)

$$C_{ij} = \frac{1}{4\pi f_{\text{sky}}} \left\{ \frac{4\pi}{l_i \Delta_i} \left[P_i^\kappa + \frac{\sigma_{\gamma_x}^2}{\bar{n}} \right]^2 \delta_{ij} + T^\kappa(\vec{l}_i, -\vec{l}_i, \vec{l}_j, -\vec{l}_j) \right\}, \quad (14)$$

where f_{sky} is the fraction of the sky surveyed, σ_{γ_x} is the per component rms intrinsic ellipticity of the sample galaxies, \bar{n} is the average galaxy number density in the survey. The first term is the sample variance; the second the shot noise. The last term, T^κ , is the trispectrum contribution, arising from non-gaussianity in the convergence field.

It is likely that a space-based deep imaging survey will offer the best prospects for probing the small scales where substructure effects are important. We adopt parameters expected for the SNAP satellite lensing survey (e.g., Massey et al. 2003): $\bar{n} = 100 \text{ gal/arcmin}^2$, $f_{\text{sky}} = 2\%$, $\sigma_{\gamma_x} = 0.34/\sqrt{2} = 0.24$.

We use the covariance of the power spectrum to perform a least-squares fitting to a fiducial model \bar{P}^κ by calculating χ^2 :

$$\chi^2 = \sum_{ij} (P_i^\kappa - \bar{P}_i^\kappa) C_{ij}^{-1} (P_j^\kappa - \bar{P}_j^\kappa), \quad (15)$$

and identify 1σ , 2σ , and 3σ contours as those with $\Delta\chi^2 = 2.30$, 6.17 , and 11.8 , respectively, which is appropriate for the two-parameter fits we will use.

We use a Λ CDM cosmological model with parameters $\Omega_m = 0.3$, $\Omega_\Lambda = 0.7$, $\Omega_b = 0.05$, $h = 0.7$, $\sigma_8 = 0.9$, and the BBKS transfer function (Bardeen et al. 1986) with the shape parameter of Sugiyama (1995).

3 RESULTS

Fig. 1 compares halo model calculations of the three-dimensional power spectrum with the non-linear fitting formula of Smith et al. (2003). In this figure, different fractions of the halo mass are placed in substructure. Adding substructure can be seen to increase power at scales $k \gtrsim 1/\text{Mpc}$.

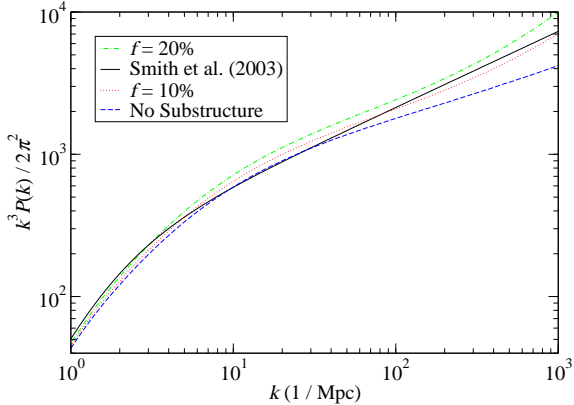


Figure 1. Halo model calculations of the dimensionless power spectrum with different fractions of the halo mass placed in NFW subhaloes. In the lower panel, we plot the dimensionless power relative to that predicted by Smith et al. (2003).

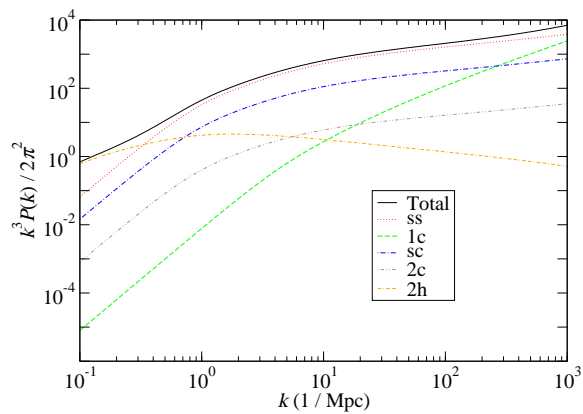


Figure 2. The dimensionless power spectrum separated into the contributions from each of the terms in Eqs. A3–A7.

Substructure models predict more power than Smith et al. for $10 \lesssim k \lesssim 100/\text{Mpc}$, but the model with 10% of the halo mass in substructure shows better agreement at smaller scales (though it should be noted that Smith et al. has been extrapolated beyond $k \gtrsim 40 h/\text{Mpc}$). The power spectrum is fairly insensitive to the exponent of the subhalo mass function, μ . Reducing μ from 0.9 to 0.7 can increase the power spectrum by about 4% at length scales $k \gtrsim 1/\text{Mpc}$.

In Fig. 2 we divide the power spectrum into contributions from the various terms in Eqs. A3–A7. The substructure contribution to the power spectrum is dominated by the smooth-subclump term, P_{sc} , on scales $k < 200/\text{Mpc}$. Thus the contribution from pairs in the same subclump, or pairs in two different subclumps, are negligible for parameter values of interest except for very high wavenumbers where baryonic effects are likely to play a role.

In Fig. 3, we leave the integral over subhalo mass uncalculated for the P_{1c} and P_{sc} terms, so that one can see

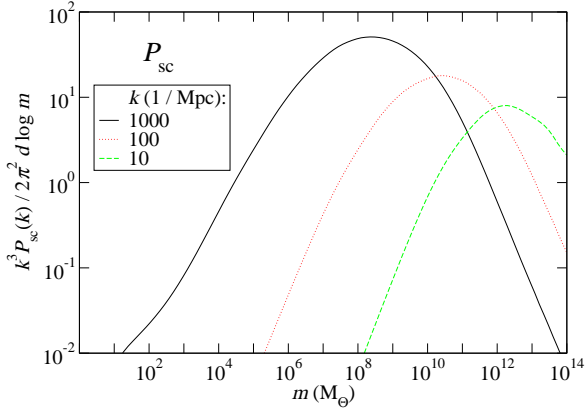


Figure 3. Contributions from the smooth-subclump term to the power spectrum per logarithmic mass bin. Integrating these curves against $d \log m$ gives $P_{sc}(k)$.

which subhalo masses provide the most power. The figures suggest that most of the extra power due to substructure between $10 \leq k \leq 100/\text{Mpc}$, comes from subhaloes of mass $10^{10} \lesssim m \lesssim 10^{12} M_\odot$. Subhaloes of this mass are likely contained in parent haloes of mass $\gtrsim 10^{12} - 10^{14} M_\odot$. Finally, since the weak lensing efficiency peaks for $z \approx 0.3 - 0.5$, the conclusion is that the weak lensing power spectrum can probe intermediate-redshift group and cluster mass haloes (provided the signal-to-noise permits its measurement as discussed below). This should make weak lensing as a probe of substructure a good complement to studies of strong lensing of quasars, which probe substructure in galactic haloes.

In Fig. 3 we plot a number of power spectra calculated with various models. Henceforth, curves titled ‘‘Bullock et al. (2001)’’ and ‘‘Huffenberger & Seljak (2003)’’ refer to halo model calculations without substructure, using the concentration parameters found in those references. It should be noted that Huffenberger & Seljak obtained their concentration parameter by fitting to Smith et al. (2003) only up to $k = 40 h/\text{Mpc}$. Both Huffenberger & Seljak and Smith et al. have been extrapolated beyond $k = 40 h/\text{Mpc}$, and the apparently poor agreement of their model with Smith et al. beyond this wavelength should be attributed to this extrapolation.

It is apparent that adding either substructure or the concentration parameter distribution affects power only on scales $k \gtrsim 10/\text{Mpc}$. The c -distribution provides a fairly constant 10% increase in power over all scales $k \geq 10/\text{Mpc}$. Substructure leads to about a 10% increase at $k = 30/\text{Mpc}$, and even more at smaller scales.

It is interesting to note that while the substructure model increases power relative to Smith et al. (2003) or Bullock et al. (2001), the concentration parameter of Huffenberger & Seljak (2003) decreases the relative power. And so, while all models may be consistent with Smith et al. at scales $k \leq 10/\text{Mpc}$, the better model should reveal itself as smaller scales are probed in higher resolution simulations and observations. If the halo model is an appropriate physical description of mass clustering, then the substructure

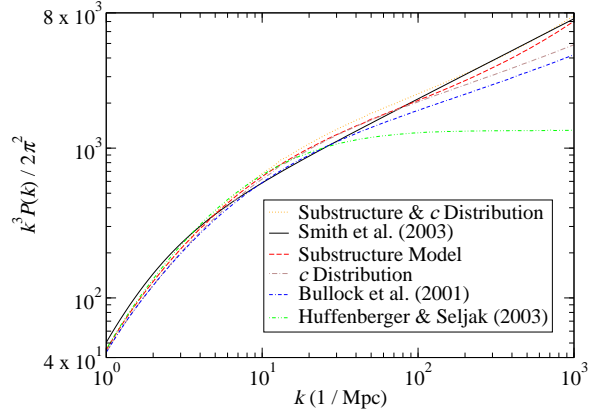


Figure 4. Comparison of dark matter power spectra predicted by various models, including substructure, a log-normal distribution of halo concentration parameters as in Eq. 10, and the non-linear fitting formula of Smith et al.

model presented here should provide the most robust predictions for the power spectrum on small scales.

In Fig. 3 we show the dimensionless convergence power spectrum predictions for the various models, assuming source galaxies at redshift one. Again, c -distribution and substructure each provide about a 10% increase in power at small scales, though the effect of substructure gets larger for the smallest scales. The halo model calculations are discrepant with Smith et al. (2003) at the 10-20% level. Most of the contribution to $P^k(l)$ for $10^3 \leq l \leq 10^5$ comes from $P(k)$ with $1 \leq k \leq 100/\text{Mpc}$. At these scales, the transition between the one-halo and two-halo terms is important. Zehavi et al. (2003) have proposed a scale-dependent correction to the bias parameter and a method to account for halo exclusion that may improve the halo model on intermediate scales. Takada & Jain (2003) employ an approximate correction for halo exclusion to obtain a more well-behaved three-point correlation function on scales $\approx 1 \text{ Mpc}$. Given the error bars expected from future surveys, it is clear that improved precision in simulations as well as model predictions is needed.

In Figs. 7 and 8, we plot the predicted three-dimensional bispectrum and convergence bispectrum. It is interesting to note that, though substructure increases the bispectra, it causes a decrease in the reduced bispectra. That is, the substructure contribution to the power spectrum factor in the denominator exceeds its contribution to the numerator in the reduced bispectrum. This is due to the fact that the dominant substructure is the smooth-subclump and the smooth-smooth-subclump term for the power spectrum and bispectrum respectively. The P_{sc} term scales as $(1 - f)f$, while the B_{sc} term scales as $(1 - f)^2f$, so the reduced bispectrum scales as $1/f$ over most scales. Thus by using both the bispectrum and power spectrum, degeneracies between the substructure fraction and other cosmological parameters can be broken. We discuss this further in Sec. 4.

Shown in Fig. 9 is the substructure contribution to the bispectrum separated into each of the terms in Eqs. A10–A15. On the scales of interest, the substructure contribu-

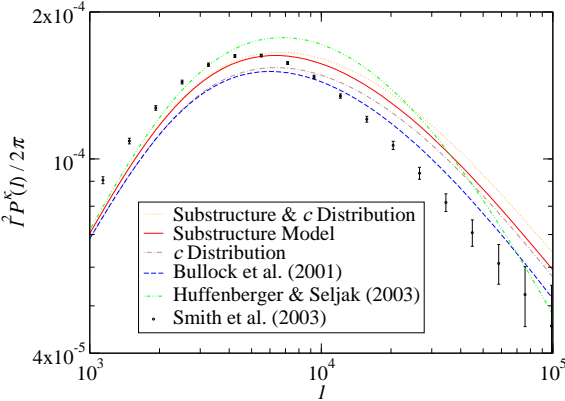


Figure 5. Various model predictions of dimensionless convergence power spectrum. Compares the substructure model and c -distribution to non-substructure models. The error bars are the diagonal part of the covariance calculated with Eq. 14 assuming $\bar{n} = 100$ gal/arcmin 2 , $f_{\text{sky}} = 2\%$, and $\langle \dot{\gamma}_{\text{int}}^2 \rangle^{1/2} = 0.34$. The trispectrum contribution to Eq. 14 is approximated by a halo model calculation.

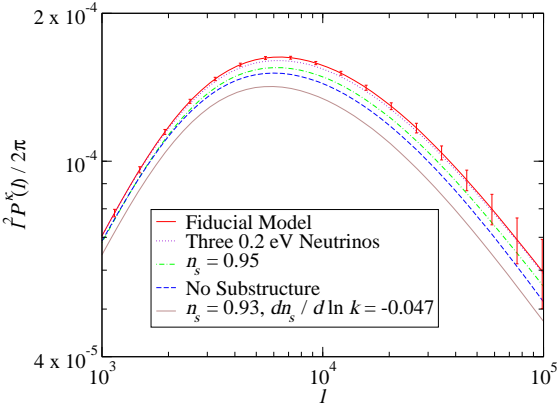


Figure 6. Dimensionless convergence power spectra for models with other phenomena that produce effects similar to substructure. The error bars are the diagonal part of the covariance calculated with Eq. 14 as in Fig. 5.

tions to the bispectrum are dominated by B_{ssc} and B_{1c} . The meaning of these terms is discussed in the Appendix. It is interesting that the bispectrum contribution from a single subhalo, B_{1c} , provides a larger contribution than the smooth component, B_{sss} , for $k \approx 10^3 \text{ Mpc}^{-1}$, but on these scales a purely gravitational calculation is not likely to be valid.

Results from the WMAP satellite have constrained the tilt and run of the primordial power spectrum. Tilt affects the small scale power in a way similar to substructure (cf. Fig. 6), so we consider next the feasibility of weak lensing to separate the effects of substructure from tilt and run in the primordial power spectrum. The results of examining the three parameter $\chi^2(f, n_s, dn_s/d \ln k)$ are shown in Fig. 3. We use the $f = 10\%$ substructure model as the fiducial model,

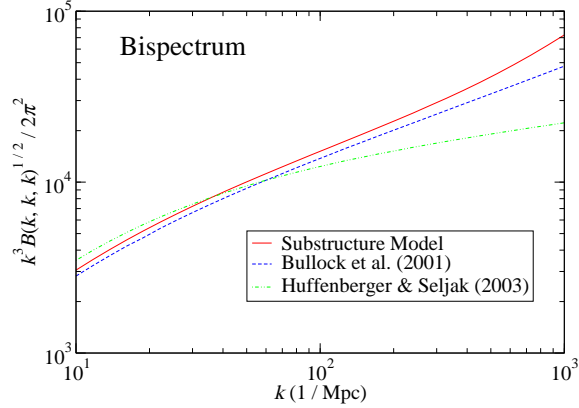


Figure 7. Various model predictions of the equilateral bispectrum. The upper panel shows the dimensionless equilateral bispectrum; the lower panel is the equilateral reduced bispectrum.

and calculate the χ^2 for $P^k(l)$ relative to the fiducial model using modes in the range $10^3 \leq l \leq 10^5$. The covariance matrix used is that in Eq. 14. In the upper panel, we assume no running and use $n_s = 1.00$ for the fiducial model. In the lower panel, we fix $n_s = 0.93$ and allow a running spectral index, as described in Spergel et al. (2003), to vary about a fiducial value of $dn_s/d \ln k = -0.047$ (Spergel et al. 2003). Note that we do not marginalize over the third parameter in these figures. We also apply priors as expected from the upcoming PLANCK mission: $\sigma_{n_s} = 0.008$ and $\sigma_{dn_s/d \ln k} = 0.004$ (Eisenstein, Hu & Tegmark 1998). These figures suggest that with CMB priors, future surveys that can measure P^k down to 0.1-arcmin scales can constrain the substructure mass fraction to about $\pm 2\%$.

4 DISCUSSION

We have shown that on small scales, the contribution of CDM substructure is important in accurate predictions of the power spectrum. In particular, it may help resolve the small scale discrepancy between N -body simulation results and the halo model. Our model with 10% substructure and a concentration parameter distribution fits the small scale

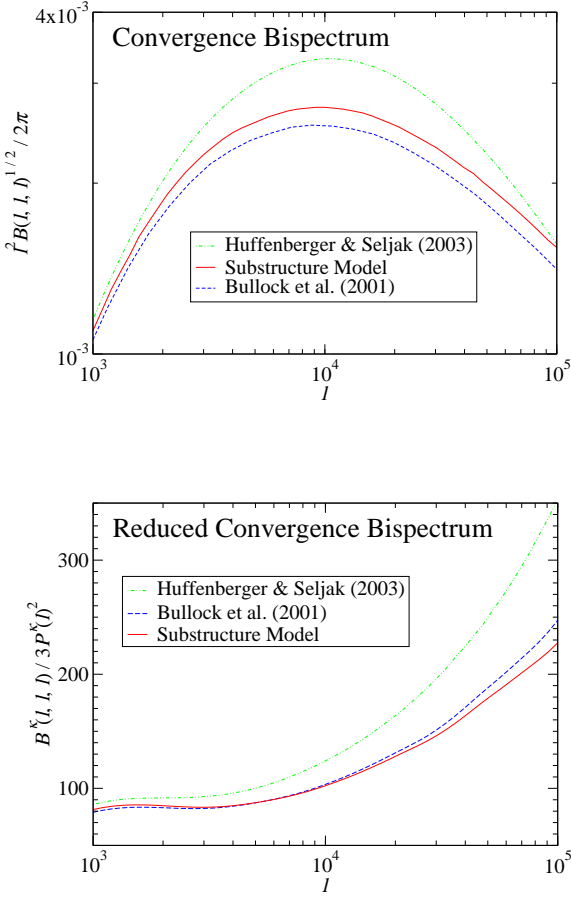


Figure 8. Various model predictions of the equilateral convergence bispectrum. Only the one-halo term is plotted. The upper panel shows the dimensionless equilateral convergence bispectrum; the lower panel is the equilateral reduced convergence bispectrum.

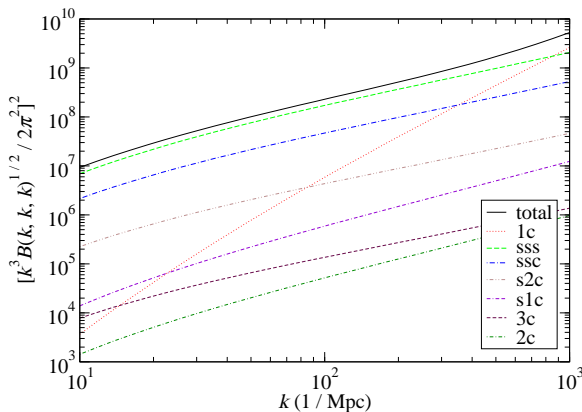


Figure 9. The one-halo term of the equilateral bispectrum separated into the contributions from each of the terms in Eqs. A10–A15.

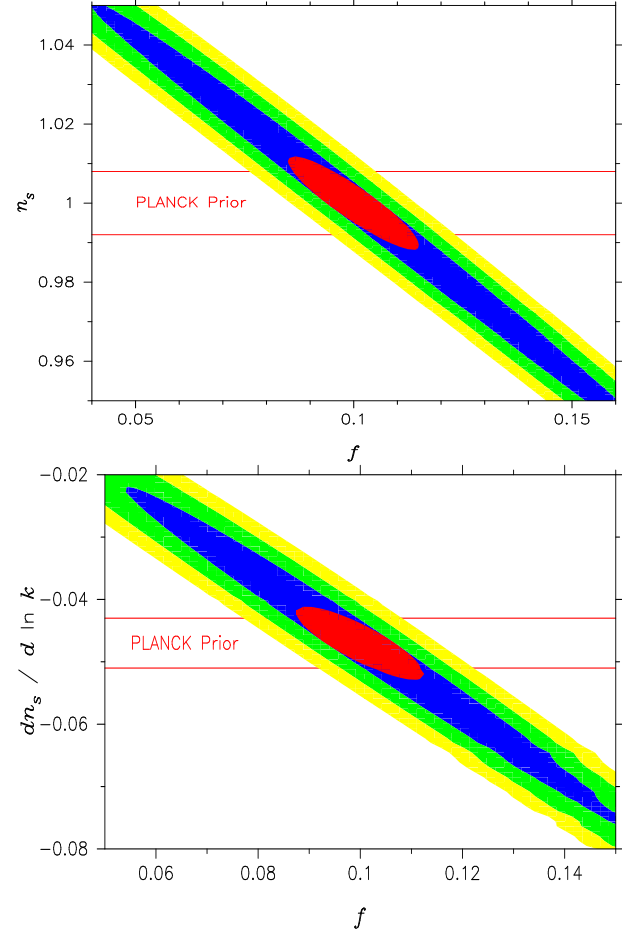


Figure 10. Contour plots on two-dimensional planes through χ^2 -space (no marginalization). In the upper panel, the spectral index and substructure mass fraction vary with no running spectral index; in the lower panel, the spectral index is fixed at $n_s = 0.93$ and a running parameter is varied along with the substructure mass fraction. The innermost contour of each plot is a one-sigma contour where we have applied prior constraints as expected from the PLANCK mission: $\sigma_{n_s} = 0.008$ and $\sigma_{dn_s / d \ln k} = 0.004$ (Eisenstein et al. 1998). The other contours are one-, two-, and three-sigma with no priors.

power spectrum extrapolated from Smith et al. (2003) quite well. Higher resolution N -body simulations are needed to test our model.

We agree with Huffenberger & Seljak (2003) that a concentration parameter distribution alone cannot resolve the discrepancy between the halo model and Smith et al. (2003). We have shown, however, that the distribution increases power on small scales by about 10%, which is comparable to the accuracy of the Smith et al. formula. Hence the scatter in the concentration parameter needs to be taken into account on scales smaller than $k = 10/\text{Mpc}$.

Our examination of the prospects for parameter constraints are by no means complete. A more careful treatment must marginalize over a larger parameter space $\chi^2(\Omega_m, \Omega_b, \Omega_\nu, \sigma_8, n_s, dn_s / d \ln k, f, \dots)$, and account for survey limitations such as intrinsic alignment of source galaxies, the limits imposed by galaxy deblending issues, and B-mode contamination. Most parameters, like Ω_m and σ_8 , are

not very degenerate with substructure, since they affect the power spectrum and bispectrum on all scales, while substructure modifies the statistics only on small scales. Such parameters can be well constrained from large scale information and probably not confuse a measurement of f . Moreover other observations constrain Ω_m and σ_8 , such as the cosmic microwave background, supernovae observations, galaxy clusters, and galaxy clustering statistics.

The situation is similar for neutrino mass and baryon fraction, though to a somewhat lesser extent. While these parameters affect the lensing power spectrum they also produce some suppression on scales with $l < 10^4$ where substructure has little effect. This will help us to constrain Ω_ν , Ω_b , and f separately. The WMAP results suggest that neutrinos are less massive than 0.2 eV (Spergel et al. 2003). We have shown that the power spectrum is much less sensitive to such neutrinos than substructure at the 10% level (Fig. 6). With regard to baryons, their abundance is well constrained from CMB data and big bang nucleosynthesis. Future observations are expected to reveal baryon oscillations in the weak lensing signal which will allow for even tighter constraints on the baryon abundance.

The effects of the parameters c_0 , β , and α , which denote the normalization and slope of the halo concentration and the inner slope of the halo profile, can be separated from substructure effects with information from the reduced bispectrum. As we noted in Sec. 3, substructure produces a proportionately larger increase in the power spectrum than in the equilateral bispectrum. The result is that substructure amplifies the power spectrum, but attenuates the reduced bispectrum. This differs from the behavior of c_0 , α , and β , as demonstrated by Takada & Jain (2003), who find that these two parameters change the power spectrum and reduced bispectrum in the same sense.

Of the parameters considered, the tilt and run of the primordial power spectrum appear to produce an effect most similar to halo substructure. Our analysis in the previous section shows that the next generation of weak lensing surveys will likely provide interesting $n_s - f$ and $dn_s/d\ln k - f$ constraints. Applying priors such as results from the PLANCK mission to these constraints should allow a detection of substructure. We find that a substructure mass fraction constraint at the $\pm 2\%$ is possible if observational errors can be controlled.

We thank Gary Bernstein and Ravi Sheth for helpful discussions. This work is supported in part by NASA through grant NAG5-10924 and NSF through grant AST03-07297.

REFERENCES

Bardeen, J. M., Bond, J. R., Kaiser, N., Szalay, A. S., 1986, *ApJ*, 304, 15.

Bartelmann, M., Schneider, P., 2001, *Physics Reports*, 340, 291.

Bullock, J. S., Kolatt, T. S., Sigad, Y., Somerville, R. S., Kravtsov, A. V., Klypin, A. A., Primack, J. R., Dekel, A., 2001, *MNRAS*, 321, 559.

Chen, J., Kravtsov, A. V., Keeton, C. R., 2003, *ApJ*, 592, 24.

Cooray, H., Hu, W., 2001, *ApJ*, 554, 56.

Cooray, A., Sheth, R., 2002, *Physics Reports*, 372, 1.

Eisenstein, D. J., Hu, W., Tegmark, M., 1998, *ApJ*, 518, 2.

Ghigna, S., Moore, B., Governato, F., Lake, G., Quinn, T., Stadel, J., 2000, *ApJ*, 544, 616.

Henry, J. P., 2001, *ApJ*, 534, 565.

Hu, W., Kravtsov, A. V., 2003, *ApJ*, 584, 702.

Huffenberger, K. M., Seljak, U., 2003, *MNRAS*, 340, 1199.

Irwin, J., Shmakova, M., 2003, *astro-ph/0308007*.

Jing, Y. P., 2000, *ApJ*, 535, 30.

Kaiser, N., 1992, *ApJ*, 388, 272.

Klypin, A., Kravtsov, A. V., Valenzuela, O., Prada, F., 1999, *ApJ*, 522, 82.

Kochanek, C. S., Dalal, N., 2003, *astro-ph/0302036*.

Limber, D. N., 1953, *ApJ*, 117, 134.

Ma, C.-P., Fry, J. N., 2000, *ApJ*, 543, 503.

Mao, S., Schneider, P., 1998, *MNRAS*, 295, 587.

Massey, R., Rhodes, J., Refregier, A., Albert, J., Bacon, D., Bernstein, G., Ellis, R., Jain, B., McKay, T., Perlmutter, S., Taylor, A., 2003, *astro-ph/0304418*.

Meiksin, A., White, M., 1999, *MNRAS*, 308, 1179.

Moore, B., Quinn, T., Governato, F., Stadel, J., Lake, G., 1999, *MNRAS*, 310, 1147.

Moore, B., Ghigna, S., Governato, F., Lake, G., Quinn, T., Stadel, J., Tozzi, P., 1999, *ApJ*, 524, L19.

Navarro, J., Frenk, C., White, S. D. M., 1997, *ApJ*, 490, 493.

Neyman, J., Scott, E. L., 1952, *ApJ*, 116, 144.

Scherrer, R. J., Bertschinger, E., 1991, *ApJ*, 387, 425.

Scoccimarro, R., Sheth, R., Hui, L., Jain, B., 2001, *ApJ*, 546, 20.

Seljak, U., 2000, *MNRAS*, 318, 203.

Sheth, R. K., Tormen, G., 1999, *MNRAS*, 308, 119.

Sheth, R. K., Jain, B., 2003, *MNRAS*, 345, 529.

Smith, R. E., Peacock, J. A., Jenkins, A., White, S. D. M., Frenk, C. S., Pearce, F. R., Thomas, P. A., Efstathiou, G., Couchman, H. M. P., 2003, *MNRAS*, 341, 1311.

Spergel, D. N., et al., 2003, *ApJS*, 148, 175.

Sugiyama, N., 1995, *ApJS*, 100, 281.

Takada, M., Jain, B., 2003, *MNRAS*, 340, 580.

Tormen, G., Diaferio, A., Syer, D., 1998, *MNRAS*, 299, 728.

White, M., 2002, *ApJS*, 143, 241.

Zehavi, M., et al., 2003, *astro-ph/0301280*.

APPENDIX A: HALO MODEL EXPRESSIONS WITH SUBSTRUCTURE

We present here the full expressions for the halo model power spectrum and bispectrum. These expressions are derived in detail in Sheth & Jain (2003).

In the halo model formalism, the power spectrum is expressed as a sum of one- and two-halo terms:

$$P(k) = P_{1h}(k) + P_{2h}(k). \quad (\text{A1})$$

We add substructure by expressing the one-halo term as

$$P_{1h} = P_{ss} + P_{sc} + P_{1c} + P_{2c}, \quad (\text{A2})$$

where

$$P_{ss}(k) = \int dM \frac{dN(M)}{dM} \left(\frac{M_s}{\bar{\rho}} \right)^2 U^2(k; M_s) \quad (\text{A3})$$

represents correlations between the smooth component of a halo. This term looks like the one-halo term of a halo model without substructure, but note that the mass of this smooth component is smaller by a fraction f , since $M_s = (1-f)M$. Hence, P_{ss} is, for all k , less than the one-halo term calculated ignoring substructure. It is up to the remaining substructure terms in Eq. A2 to make up for this loss.

$$P_{sc}(k) = 2 \int dM \frac{dN(M)}{dM} \frac{M_s}{\bar{\rho}} U(k; M_s) U_c(k; M_s) \int dm \frac{dn(m; M)}{dm} \frac{m}{\bar{\rho}} u(k; m) \quad (\text{A4})$$

denotes correlations between the smooth component and a subclump. The factor of 2 arises because either of the two density elements of the two-point function may lie in a subclump.

$$P_{1c}(k) = \int dM \frac{dN(M)}{dM} \int dm \frac{dn(m; M)}{dm} \left(\frac{m}{\bar{\rho}} \right)^2 u^2(k; m) \quad (\text{A5})$$

represents correlations where both elements lie in the same subclump, and

$$P_{2c}(k) = \int dM \frac{dN(M)}{dM} U^2(k; M_s) \left[\int dm \frac{dn(m; M)}{dm} \frac{m}{\bar{\rho}} u(k; m) \right]^2 \quad (\text{A6})$$

describes correlations between different subclump. Though this expression assumes that subclumps obey a Poisson distribution, we do not consider it important since this contribution to the power spectrum is subdominant (see Fig. 2).

Finally,

$$P_{2h}(k) = \int dM_1 \frac{dN(M_1)}{dM_1} \frac{M_1}{\bar{\rho}} U(k; M_1) \int dM_2 \frac{dN(M_2)}{dM_2} \frac{M_2}{\bar{\rho}} U(k; M_2) P(k; M_1, M_2) \quad (\text{A7})$$

is the two-halo term. Note that we have ignored substructure for this contribution: on large scales we trust the approximation of smooth NFW haloes with no substructure.

The one-halo term of the bispectrum has a similar division:

$$B_{1h} = B_{sss} + B_{ssc} + B_{s1c} + B_{s2c} + B_{1c} + B_{2c} + B_{3c}. \quad (\text{A8})$$

$$B_{sss}(k_1, k_2, k_3) = \int dM \frac{dN(M)}{dM} \left(\frac{M_s}{\bar{\rho}} \right)^3 U(k_1; M_s) U(k_2; M_s) U(k_3; M_s) \quad (\text{A9})$$

is the contribution with all three density elements from, or the vertices of the triangle in, the smooth component of a halo.

$$B_{ssc}(k_1, k_2, k_3) = \int dM \frac{dN(M)}{dM} \left(\frac{M_s}{\bar{\rho}} \right)^2 U(k_1; M_s) U(k_2; M_s) U_c(k_3; M_s) \int dm \frac{dn(m; M)}{dm} \frac{m}{\bar{\rho}} u(k_3; m) + \text{cyclic } k_i \text{ permutations} \quad (\text{A10})$$

places only one vertex of the triangle in a subclump.

$$B_{s1c}(k_1, k_2, k_3) = \int dM \frac{dN(M)}{dM} \frac{M_s}{\bar{\rho}} U(k_1; M_s) U_c(k_1; M_s) \int dm \frac{dn(m; M)}{dm} \left(\frac{m}{\bar{\rho}} \right)^2 u(k_2; m) u(k_3; m) + \text{cyclic } k_i \text{ permutations} \quad (\text{A11})$$

has one vertex in the smooth component and the other two in the same subclump.

$$B_{s2c}(k_1, k_2, k_3) = \int dM \frac{dN(M)}{dM} \frac{M_s}{\bar{\rho}} U(k_1; M_s) \prod_{i=2}^3 U_c(k_i; M_s) \int dm_i \frac{dn(m_i; M)}{dm} \frac{m_i}{\bar{\rho}} u(k_i; m_i) + \text{cyclic } k_i \text{ permutations} \quad (\text{A12})$$

has one vertex in the smooth component and the other two in different subclumps.

$$B_{1c}(k_1, k_2, k_3) = \int dM \frac{dN(M)}{dM} \int dm \frac{dn(m; M)}{dm} \left(\frac{m}{\bar{\rho}}\right)^3 u(k_1; m) u(k_2; m) u(k_3; m) \quad (\text{A13})$$

places all three vertices in the same subclump.

$$\begin{aligned} B_{2c}(k_1, k_2, k_3) &= \int dM \frac{dN(M)}{dM} U_c^2(k_1; M_s) \int dm_1 \frac{dn(m_1; M)}{dm_1} \frac{m_1}{\bar{\rho}} u(k_1; m_1) \\ &\times \int dm_2 \frac{dn(m_2; M)}{dm_2} \left(\frac{m_2}{\bar{\rho}}\right)^2 u(k_2; m_2) u(k_3; m_3) + \text{cyclic } k_i \text{ permutations} \end{aligned} \quad (\text{A14})$$

divides the three vertices between two subclumps.

$$B_{3c}(k_1, k_2, k_3) = \int dM \frac{dN(M)}{dM} \prod_{i=1}^3 U_c(k_i; M_s) \int dm_i \frac{dn(m_i; M)}{dm_i} \frac{m_i}{\bar{\rho}} u(k_i; m_i) \quad (\text{A15})$$

places the three vertices in different subclumps.